The complementary structural studies of the double metal cyanide type catalysts for the ring opening polymerization of the oxiranes*)

Arkadiusz Chruściel[1), **)], Wiesław Hreczuch[1)], Krystyna Czaja[2)], Krystyna Ławniczak-Jabłońska[3)], Jarosław Janik[1)]

DOI: dx.doi.org/10.14314/polimery.2016.421

Abstract: The extensive complementary experimental studies of the double metal catalysts (DMC) with two kinds of the organic ligands were performed. The chemical justification of the observed TG/DSC (thermogravimetric analysis/differential scanning calorimetry) steps was proposed. Several organic ligand complexing states were found in both types of catalysts. X-ray absorption spectroscopy (XAS) analysis established that only Zn atoms are the active metallic centers in DMC catalyst regardless the used ligand. Cl atoms were detected near some of Zn atoms. Contrary to the common suppositions no significant amount of oxygen atoms was detected in the closest coordination spheres of Zn.

Keywords: double metal cyanide catalysts (DMC), thermal analysis, thermogravimetric analysis (TG), differential scanning calorimetry (DSC), evolved gas analysis (EGA), X-ray absorption spectroscopy (XAS), X-ray absorption near edge structure (XANES), extended X-ray absorption fine structure (EXAFS).

Komplementarne badania strukturalne dimetalocyjankowych katalizatorów polimeryzacji z otwarciem pierścienia oksiranowego

Streszczenie: Przeprowadzono badania strukturalne katalizatorów dimetalocyjankowych (DMC) z dwoma rodzajami ligandów organicznych. Zaproponowano wyjaśnienie etapów przebiegu krzywych otrzymanych metodą analizy termograwimetrycznej i różnicowej kalorymetrii skaningowej (TG/DSC) badanych katalizatorów. Wykazano obecność kilku stopni związania ligandów w kompleksach DMC. Na podstawie wyników badań z wykorzystaniem absorpcji rentgenowskiej (XAS) stwierdzono, że centrum aktywne katalizatora stanowi atom cynku. W bezpośrednim sąsiedztwie atomów Zn wykryto obecność atomów Cl, natomiast w najbliższych sferach koordynacyjnych atomu Zn nie wykryto atomów tlenu.

Słowa kluczowe: katalizatory dimetalocyjankowe (DMC), analiza termiczna, analiza termograwimetryczna (TG), różnicowa kalorymetria skaningowa (DSC), analiza wydzielanych gazów (EGA), rentgenowska absorpcyjna spektroskopia struktury przykrawędziowej (XANES), synchrotronowa absorpcyjna spektroskopia rentgenowska (EXAFS).

Polymerization of the oxirane molecules, preceded by the oxirane ring catalytic opening step, is usually carried out with oxirane (1,2-epoxyethane, ethylene oxide) or methyloxirane (1,2-epoxypropane, propylene oxide). A general reaction equation, based on the example of the addition of methyloxirane to the hydroxyl group incorporated into the molecule called "starter", is shown in Scheme A.

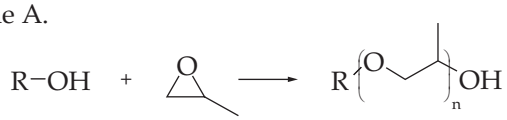

where: R = hydrogen or alkyl

Scheme A

Conventional catalysts for epoxy ring opening have been known for a long time; typically alkaline compounds, they are usually introduced into a reaction medium as hydroxides (NaOH, KOH). The main commonly observed disadvantage of the alkaline catalyst is the significant number of unfavorable side processes occurring

[1)] MEXEO Institute of Technology, Energetyków 9, 47-225 Kędzierzyn-Koźle, Poland.

[2)] University of Opole, Faculty of Chemistry, Oleska 48, 45-052 Opole, Poland.

[3)] Institute of Physics, Polish Academy of Sciences, Lotników 32/46, 02-668 Warsaw, Poland.

*) Material contained in is article was presented at 58th Annual Scientific Meeting of the Polish Chemical Society, 21–25 September 2015, Gdansk, Poland.

**) Author for correspondence; e-mail: arkach@mexeo.pl

in their presence, leading both to a product with a broad distribution of homologues as well as the occurrence of competitive rearrangement reactions.

The implementation of double metal cyanide type (DMC) catalysts [1–3] to the industrial praxis in 1960's was a milestone step in the development of the epoxide ring opening polymerization technology.

The DMC catalysts show **exceptionally** high activity, which is their unique feature.

An active matter in a typical state-of-the-art DMC catalyst is usually a multiphase, nonstoichiometric compound, the chemical composition of which may be defined by the general formula $Me^1_x[Me^2(CN)_6]_y \cdot L^1_{a_1} \cdots L^n_{a_n}$, where Me^1 denotes a first metal ion from the group of bivalent transition metals, Me^2 denotes a second metal ion from the group of multivalent transition metals (above +2), the symbol $L^1 \cdots L^n$ denotes potential complexing ligands such as halides, hydroxides, sulfates, and/or numerous organic heteroatom-containing compounds, which determine the catalytic properties of DMC catalysts, whilst the x, y, $a_1 \ldots a_n$ are non-stoichiometric ones.

The active matter of the frequently used industrial DMC catalysts consists of a complex bonding of zinc as a Me^1 metal, cobalt as Me^2 and *tert*-butanol or 1,2-dimetoxyethane (glyme) as organic ligands.

Although the DMC catalysts have been effectively used for decades, knowledge of the molecular factors determining their remarkably high activity and selectivity remains poor. Attempts at a structural explanation of the properties of DMC catalysts are based on the experimental verification of the hypothesis that the activity of DMCs is dictated by the properties of Me^1 metal (most frequently Zn) through the formation of a coordination bond with an organic co-ligand oxygen atom which is weaker than the strong Zn-N bond [2–9]. This seems to be justified both in the light of the coordination properties of Zn [10] and, on the other hand, the commonly known stability of the hexacyanometallate ion [11].

Unfortunately, no sufficiently unambiguous experimental data on the structural nature of active centers, the nature of so-called organic ligands and their role in DMC catalysts have been communicated as yet. What is more, no satisfactory experimental evidence for the presence of Zn-organic ligand coordination bonds has been established. In other words, no specific for the catalyst phase analytical signal were identified until now.

Observable features of the molecular structure of DMC catalysts and their catalytic properties are limited only to the application of X-ray powder diffraction (XRD), infrared spectrophotometry, and X-ray photoelectron spectroscopy (XPS). However, the above mentioned techniques are mainly used to confirm the identity of the obtained DMC material. Results of the application of XRD have been reported by a number of authors [4–9, 12–15] but XRD provides information related only to crystalline fraction of material. The method enabled the discovery of a relationship between the quantity of the amorphous phase and their activity.

No unambiguous spectral effects, characteristic for catalytically active Zn atoms centers, have been differentiated using IR spectrophotometric studies of DMC catalysts. Although some obvious characteristic absorption ranges were found which correspond to the specific valence vibrations, no explicit interpretation for the presence of catalytic centers (Zn weakly bonded) has been found [4, 8, 14, 15].

An equally important issue for DMC development is the role of the organic component in the formation of active matter and the ring-opening mechanism. A commonly claimed point of view regarding the role of the organic component is based on the supposition of its active action during the catalytic process through its simple substitution as the supposed ligand bonded coordinatively directly with the Zn atom by oxirane and/or the starter molecule [4, 5, 8, 9].

However, the question remains open, in the light of the observation made by the present authors recently with the use of extended X-ray absorption fine structure (EXAFS) analysis of DMC catalysts, showing that oxygen atoms in organic ligands remain at a relatively far distance from Zn atoms beyond the range which is typical of the coordination bonds [16, 17].

Valuable sources of information supporting investigation on the structure and mechanism of the activity of catalysts are those connected with their thermal behavior. The relatively high volatility of organic ligands seems to be useful for thermal analysis, making possible both the detection of several forms of the ligand bonding and their quantitative evaluation.

The number of papers reporting the application of thermal analysis techniques in the examination of DMC catalysts is rather moderate. Generally, they are not focused on DMC thermal behavior and the thermograms (mainly TG) are used as fingerprint patterns, specific to any kind of catalyst [18–21].

An interesting direction of the attempts on the structural justification of the catalytic properties of the DMC catalysts is the application of molecular modeling with the use of *density functional theory* (DFT) computations [22, 23]. However, the reports on this subject are still few in number, the results of theoretical investigations could be an important complement to the conclusions of experimental research.

The paper presents an extensive complementary experimental studies of DMC catalysts. The general goal of these investigations performed with the use of numerous physical methods to examine the structure of matter, as the X-ray absorption spectroscopy (XAS) and thermal analysis was to shed new light on the problem of the unknown structural factors determining the catalytic properties of the subject materials. Particularly, the studies were focused on the detection of the analytical signals connected with the catalytic phase of the DMC material, the thermal behavior of the ligand in catalyst complex and the constitution of the catalytic center.

EXPERIMENTAL PART

Materials

tert-Butyl alcohol (*t*-BuOH, > 99 % pure) was obtained from Brenntag, Kędzierzyn–Koźle, Poland.

$K_3[Co(CN)_6]$ was a commercial product prepared in MEXEO, Kędzierzyn-Koźle, Poland.

Acrylic acid polyamide − Rokrysol WF2 (content of 5.6 % m/m) – used as a flocculant, was purchased from Brenntag, Kędzierzyn–Koźle, Poland.

Preparation of DMC materials

The samples of DMC-1—DMC-5 catalysts containing *tert*-butanol as an organic ligand were prepared according to the method described elsewhere [3].

Sample DMC-0, being the "pure" trizinc *bis*-[hexacyanocobaltate(III)] $Zn_3[Co(CN)_6]_2 \cdot nH_2O$, was prepared as mentioned above, without adding the ligand.

Methods of testing

Catalysts performance tests

The confirmation of the catalytic performance of both catalysts was done according to the procedure described in [3].

Analysis of Co and Zn

The Solar M6 Thermo flame atomic absorption spectrometer equipped with the Co (240.7 nm) and Zn (213.9 nm) hollow cathode lamps was used to analyze quantitatively Co and Zn in the DMC catalyst samples.

A deuterium lamp was applied for the background correction. The air/C_2H_2 gas was used.

The SPS-SW2 Batch 123 material was used for calibration.

The weighed amount of *ca.* 0.1 g of the catalyst was dissolved in 6M HCl, then diluted to 100 cm^3 with 1 : 1 HCl.

0.5 cm^3 of the solution was then diluted to 50 cm^3 with distilled water and analyzed.

A calibration curve method was employed to estimate concentrations for both metals.

Analysis of N and C

The Vario EL III CHNOS Elemental Analyzer was used to determine the total carbon and nitrogen in the DMC catalyst samples.

X-ray absorption spectrometry (EXAFS/XANES analysis)

The local atomic structure around Zn and Co atoms was determined by EXAFS.

Experiments were performed at beam line SAMBA of the Soleil (Paris/France) synchrotron. Appropriate amounts of the samples were mixed with cellulose and pressed into a pellet. The samples were measured in air, in transmission geometry at room temperature. The analysis was performed using IFEFFIT package.

TGA/EGA-FTIR, MS, and DSC analysis

Mettler Toledo TGA/DSC1 thermoanalytical system coupled with mass spectrometer was used for TGA and EGA analysis.

Independent DSC thermograms were measured with using a Mettler Toledo DSC1 differential scanning calorimeter.

TGA/EGA measurement parameters: carrier gas – N_2, 20 cm^3/min; open Al_2O_3 crucible.

DSC measurement: carrier gas – N_2, 30 cm^3/min; open Al crucible.

Mettler Toledo STAR^e 12.00 software was used for data processing.

RESULTS AND DISCUSSION

Elemental analysis of the examined DMC materials

Table 1 and Table 2 show the results of elementary analysis for carbon, nitrogen, cobalt and zinc in the test materials: DMC-0 showing no catalytic properties, and DMC-1 to DMC-10 containing *t*-BuOH or glyme as the organic ligand – showing confirmed, comparable catalytic properties in methyloxirane polymerization reaction (see the previous text), and assessment of nitrogen/cobalt molar ratios. The values of variability coefficients for the quantitative parameters determined as a ratio between standard deviation concentration for the respective elements and their arithmetic average indicate a relatively good repeatability of their elemental composition for each catalyst group.

The remarkable feature of the established values of elemental composition characteristics is an approximately constant nitrogen/cobalt molar ratio, corresponding to the stoichiometric ratio of the two elements in the hexacyanocobaltate(III) ion (6 : 1). The values of that ratio are characterized by a rather high stability, which results from the constancy of composition of a particularly stable $[Co(CN)_6]^{3-}$ ion and is a measure of repeatability of synthesis of the catalyst.

Because there is an intentional excess of zinc in relation to cobalt in the DMC catalysts, as compared with stoichiometric relationships observed in zinc hexacyanocobaltate(III), the molar ratio Zn : Co in DMC-1–10 samples exceeds the value 3 : 2 and is about 2 : 1, regardless of the type organic ligand.

Also the carbon/nitrogen ratio is higher than 1 : 1 due to the presence of the organic component. Obviously, that ratio is conserved for sample DMC-0, the "pure" zinc hexacyanocobaltate(III), and is 1 : 1.

T a b l e 1. Results of elemental analysis for samples of reference $Zn_3[Co(CN)_6]_2$ (DMC-0) and DMC catalysts containing *t*-BuOH ligand (DMC-1–DMC-5)

Sample	[C], wt %	[N], wt %	[Co], wt %	[Zn], wt %	n_N/n_{Co}	n_{Zn}/n_{Co}	n_C/n_N
DMC-0	14.55	16.95	11.79	18.87	6.05	1.45	1.00
DMC-1	24.92	17.83	11.67	26.35	6.43	2.04	1.63
DMC-2	24.99	17.04	12.43	28.42	5.77	2.07	1.71
DMC-3	23.80	17.46	12.10	27.80	6.07	2.08	1.59
DMC-4	22.44	16.44	11.52	29.77	6.01	2.34	1.59
DMC-5	22.13	17.71	12.55	24.21	5.94	1.74	1.46
Average	23.66	17.30	12.05	27.31	6.04	1.95	1.50
Standard deviations	1.34	0.57	0.45	2.12	0.24	0.31	0.26
CV, %	5.67	3.27	3.76	7.78	4.02	15.9	17.1

CV – variability coefficients;
[C] – total carbon concentration in DMC material, wt %;
[N] – total nitrogen concentration in DMC material, wt %;
[Co] – total cobalt concentration in DMC material, wt %;
[Zn] – total zinc concentration in DMC material, wt %;
n_N/n_{Co} – molar ratio of nitrogen and cobalt in DMC material, mol/mol.
n_{Zn}/n_{Co} – molar ratio of zinc and cobalt in DMC material, mol/mol;
n_C/n_N – molar ratio of carbon and nitrogen in DMC material, mol/mol.

T a b l e 2. Results of elemental analysis for samples DMC-6–DMC-10 containing glyme ligand

Sample	[C], wt %	[N], wt %	[Co], wt %	[Zn], wt %	n_N/n_{Co}	n_{Zn}/n_{Co}	n_C/n_N
DMC-6	25.39	17.63	12.31	23.73	6.03	1.75	1.68
DMC-7	22.12	15.61	10.95	24.59	6.00	2.03	1.65
DMC-8	26.37	17.53	11.82	23.07	6.24	1,77	1.76
DMC-9	23.25	16.40	11.24	24.78	6.14	2.00	1.65
DMC-10	23.38	16.35	11.39	23.96	6.04	1.91	1.67
Average	24.10	16.70	11.54	24.03	6.09	1.89	1.68
St.dev.	1.73	0.86	0.53	0.69	0.10	0.13	0.05
CV, %	7.18	5.14	4.61	2.86	1.63	6.79	2.70

T a b l e 3. The local atomic order around Zn atoms in the hydrated reference material, and both catalysts

Shell*)	Elem.	Reference material			DMC-*t*-BuOH			DMC-glyme		
		100 %			84 (3) %			79 (5) %		
		No	*R*, Å	$Sigma^2$	No	*R*, Å	$Sigma^2$	No	*R*, Å	$Sigma^2$
1	6 N 2.090 Å	6	2.09 (4)	0.013 (1)	N 3.36	1.974 (3)	0.003 (1)	N 3.16	1.98 (1)	0.005 (1)
2	6 C 3.23 Å	6	3.23 (1)	0.006 (2)	C 3.36	2.98 (2)	0.013 (4)	C 3.16	3.00 (1)	0.009 (3)
3	24 O 4.23 Å	3 (1)	4.50 (6)	0.008 (6)	Co 1.68	5.006 (4)	0.004 (1)	Co 1.58	5.00 (1)	0.007 (1)
4	6 Co 5.12 Å	6	5.15 (8)	0.018 (8)	Co 1.68	5.038 (4)	0.004 (1)	Co 1.58	5.04 (1)	0.007 (1)
Zn-Cl										
1	Cl	0			0.40 (2)	2.24 (1)	0.003 (1)	0.56 (5)	2.24 (1)	0.005 (1)
R_f		0.013			0.003			0.018		

*) In first column the number of considered sphere around Zn is given, in second column the kind and number of atoms and distance as resulted from crystallographic data is provided for comparison, in the subsequent columns number of atoms (No) in the given coordination sphere, distance (*R*) from Zn atom in Å, and Debye – Waller factors ($Sigma^2$) as resulted from performed analysis is listed. In the parentheses the confidence interval indicated by IFEFFIT code is given. R_f factor indicate the quality of the fitting.

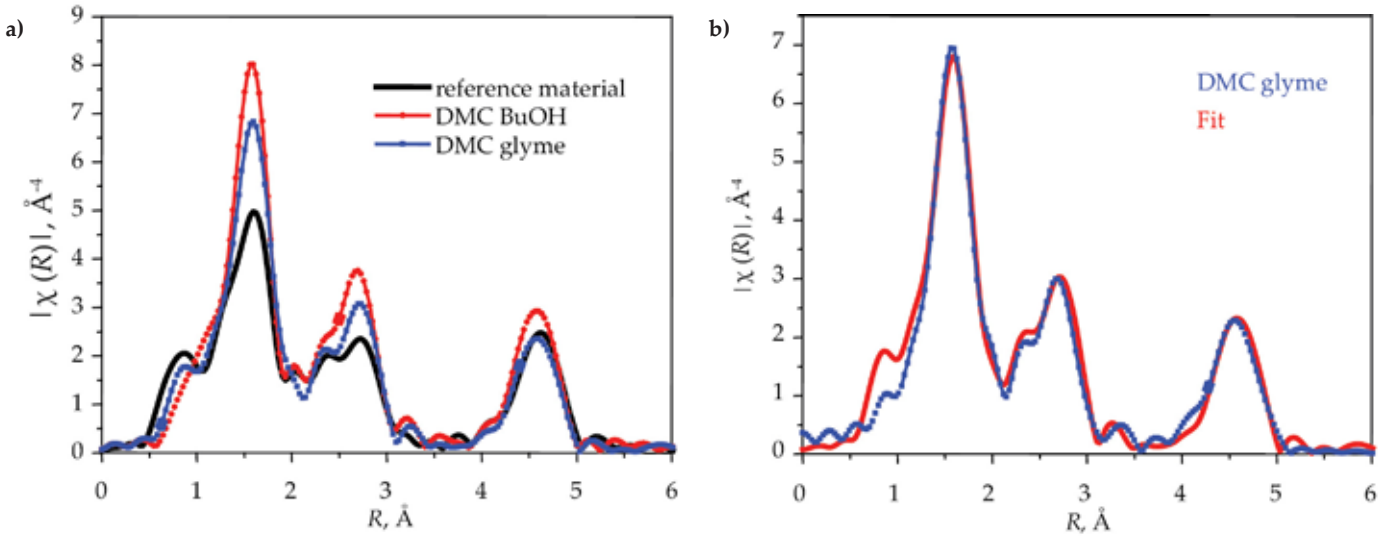

Fig. 1. Zn K-absorption edges: a) Fourier transform at module of the EXAFS spectra of the considered catalysts, b) fit to the EXAFS data of the model for DMC-glyme

X-ray absorption

EXAFS analysis provide information about local atomic structure around given atoms. All given atoms are examined as well these located in amorphous as in crystalline structure. The atomic orders around Zn and Co atoms were investigated by measuring the spectra of K-edges of Zn and Co. The spectra of Zn atoms differ for the analyzed materials (Fig. 1a). To analyze the measured spectra the appropriate models of atomic order should be constructed. Next the theoretical spectra for this model were simulated and compared with experiment. During the analysis several models of atomic order around Zn were considered, taking into account the models proposed in the literature discussing the role of O and Cl atoms in DMC catalysts [6, 8, 22, 23].

The best fit to the EXAFS data was obtained for the model assuming that considerable fraction of Zn atoms in catalyst have the local atomic order as should be in the reference anhydrous material with rhombohedral structure (Zn bond to 4 cyanide groups) and some of them have Cl in the first coordination sphere. The example of such fit is shown in Fig. 1b for DMC glyme and numerical value of fits are listed in Table 3. In hydrated reference material [zinc hexacyanocobaltate(III)] the Zn atoms are bonded to 6 cyanide groups.

EXAFS analysis confirmed the intentional access of Zn atoms as compare to crystalline anhydrous material. It was found that only 84 (3) % and 79 (5) % of Zn atoms have 4 near neighbour CN^- groups for DMC *t*-BuOH and DMC glyme, respectively. Moreover, in the first coordination sphere 0.4 and 0.56 Cl atom per one Zn atom in the distance 2.24 Å, respectively, was identified for investigated catalysts. This Zn-Cl bond length is close to that in $ZnCl_2$ (2.30 Å), therefore can be considered as characteristic for Zn-Cl bond. Nevertheless, the model with the atomic order characteristic for $ZnCl_2$ (in first

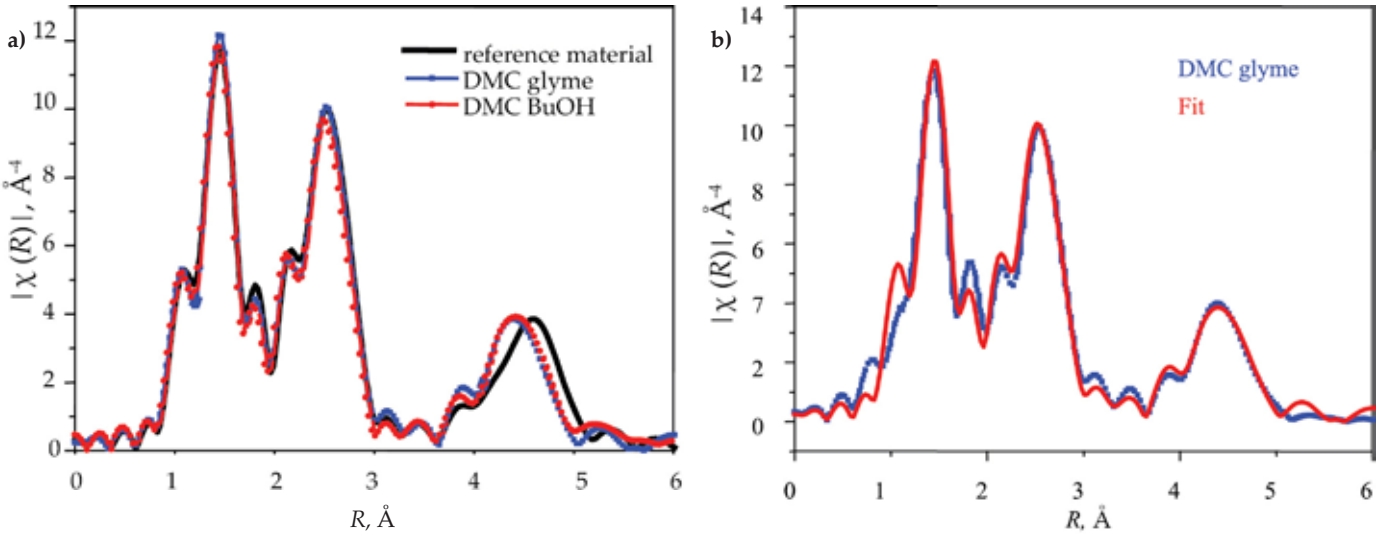

Fig. 2. Co K-absorption edges: a) Fourier transform at module of the EXAFS spectra of the considered catalysts, b) fit to the EXAFS data of the model for DMC-glyme

coordination shell 2 Cl in distance 2.3 Å and 2 Cl in distance 3.2 Å and next 4 Zn atoms at distance 3.75 Å and 2 Cl in distance 3.8 Å) could not be fitted. Consequently, the existence of $ZnCl_2$ compound was not confirmed. The example of the best fit of model to experimental spectra is shown in Fig. 1b for DMC glyme. To be sure that only Cl atoms can be located close to Zn atoms the model with oxygen was considered. Such model cannot be fitted to experimental data. Therefore, the attempt was performed to substitute some of Cl atoms with oxygen. This model gave an increase of the errors of estimated parameters and an increase of the R_f parameter which estimates the quality of the fit. Nevertheless, one cannot exclude that oxygen atoms can be bonded to Zn but in the very limited amount. In many reports it is emphasized that the type (coming from water or ligands) and amount of oxygen atoms coordinated to Zn should play an important role in the ring opening polymerization of propylene oxide since oxygen atoms coordinated to a zinc ion are believed to be a real active center of DMC catalyst [15, 23]. From the performed EXAFS studies we cannot confirm this role. Instead we do confirm the location of Cl close to Zn atoms. The role of Cl is also discussed in the literature on the base of XPS experiment [8] and molecular calculation [22]. In the paper by Zhang *et al*. [8] based on overall chemical premises the role of Cl atoms in the catalytic properties of DMC was postulated and reported that the ligand influences on catalytic activity only by helping to form the amorphous structure.

The local atomic structure around Co atom was practically not changing for all investigated materials as can be seen in Fig. 2a.

In performed fits for given catalyst the increase in the number of oxygen atoms in distance 3.10 Å and 4.62 Å were only noticed. The oxygen atoms can originate from water molecule or ligand. The error indicated by IFEFFIT code for the number of these atoms is quite large indicating that oxygen can be distributed non-homogeneously. This confirms that Co metallic center is not active during the catalyst preparation. Interestingly, the atomic order around Co remains like in hydrated form of $Zn_3[Co(CN)_6]_2{\cdot}nH_2O$ with cubic (*Fm*-3*m* group) structure. Therefore, in catalyst both metals have different atomic order. Zn atoms like in anhydrous structure (rhombohedral *R*3*c* group) bonded with four CN^- groups and Co atoms like in hydrated structure bonded with six CN^- groups. In Fig. 2b as an example of fitting for Co atoms, the fit for DMC glyme is shown.

Qualitative thermal analysis of DMC materials

Zinc hexacyanocobaltate(III)

Figure 3 shows typical TG/DTG and DSC curves for a sample of trizinc *bis*-[hexacyanocobaltate(III)].

The curves show the presence of a noticeable mass loss step which is typical of the liberation of water appearing in the range 25–90 °C. That step is accompanied by a mass loss of 21.6 %. Although that step may occur due to the liberation of crystallization water, the quantity of water that is liberated in that temperature range does not correspond to the expected crystallographic value, which is typical of dodecahydrate (26 %) [24], but varies over a relatively wide range 5–21 %. This is in agreement with EXAFS analysis of reference hydrated material (Table 3) where only three oxygen atoms were detected instead of 24 resulted from perfectly hydrated trizinc *bis*-[hexacyanocobaltate(III)].

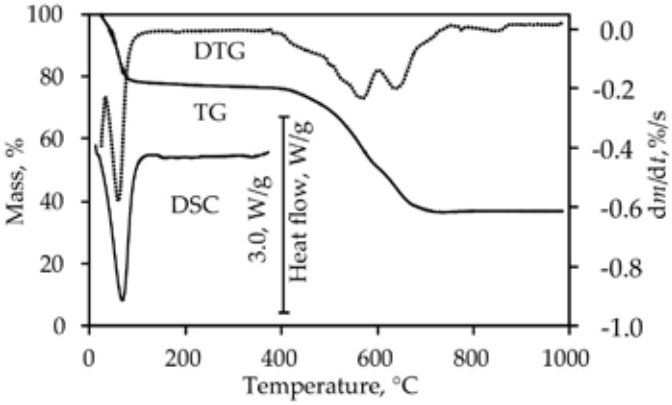

Fig. 3. TG/DTG and DSC curves of trizinc *bis*-[hexacyanocobaltate(III)]

A strong endothermal effect occurs in the DSC curve profile in that temperature range. The value of enthalpy of evaporation for the component, as found from the DSC peak integration and value of mass loss, previously established by the present authors for 5 different samples of that compound, was -2440 ± 190 J/g of liberated mass and is statistically indistinguishable from the average literature value of water evaporation enthalpy in the temperature range 25–110 °C (-2330 J/g).

At temperatures above 90 °C, its further increase to *ca*. 400 °C leads only to a minor linear mass loss by 1.93 %, running at an approximately constant rate.

After the value of about 350 °C is reached, an intense, multi-step process of mass loss commences, which is described quantitatively in Table 4. The thermal decomposition residue is 36.55 %.

The EGA-FTIR spectra for gaseous decomposition products has enabled interpretation of the mass loss steps in the aspect of the physical-chemical processes taking place.

Figure 4 shows a 3D thermogram of the test sample of zinc hexacyanocobaltate(III) in the space delineated by absorbance-wave number-temperature.

In the range of 25–150 °C, the two intensive oscillating-shaped maxima are observed: in the range of 4000––3500 cm^{-1} and 2000–1300 cm^{-1}, respectively. Both were identified as characteristic for water molecule vibration. According to the earlier observed profile of the TG/DTG curves, absorbance in those wave number regions decreases after reaching its maximum at temperatures in the range 50–60 °C, which is connected with the nearly

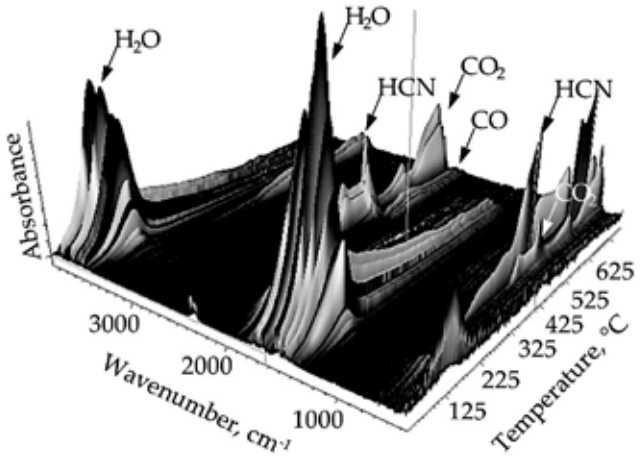

Fig. 4. EGA-FTIR thermogram of trizinc *bis*-[hexacyanocobaltate(III)]

complete evaporation of water.

The effect of decomposition of zinc hexacyanocobaltate(III), which was observed earlier for the less sensitive TG measurement only in the region 320–350 °C, occurred in the 3D thermogram still before reaching 300 °C as an increase in absorbance with temperature in the wave number ranges 3450–3250 cm^{-1} and 800–600 cm^{-1}, in which absorption bands appear, identified as the hydrogen cyanide absorption bands.

Hydrogen cyanide emission is observed at temperatures from *ca*. 300 °C up to the end of the thermogram at *ca*. 800 °C, and may be the result of the gradual consecutive detachment of the respective cyanide ions in the hexacyanocobaltate(III) ion structure.

Detection of the presence of hydrogen cyanide in gaseous products of decomposition of the zinc hexacyanocobaltate(III) sample, which should contain no moisture due to its evaporation in the temperature range 25–110 °C, indicates the possibly incomplete evaporation of the crystallization water which potentially carried the hydrogen atoms present in the hydrogen cyanide, as well as the possibility that a reaction took place between water and the hexacyanocobaltate ion. Taking into consideration the charge conservation law, the hypothetical reaction between water and the hexacyanocobaltate(III) ion leading to the formation of hydrogen cyanide can be described by Scheme B:

$$[Co(CN)_6]^{3-} + H_2O \rightarrow [Co(CN)_5OH]^{3-} + HCN$$

Scheme B

Another possible zinc hexacyanocobaltate(III) decomposition process involves oxidation of cyanides to form carbon dioxide leading, in effect, to CO_2 emission which is observed at *ca*. 350 °C and higher temperatures as the appearance of CO_2 – specific absorption maximum groups in the wave number ranges 2400–2250 cm^{-1}, and a narrow absorption band, corresponding to the wave number of about 680 cm^{-1}.

DMC-*t*-BuOH catalysts (samples DMC-1–DMC-5)

Figures 5 and 6 show the thermograms of the DMC catalysts prepared with the use of *tert*-butanol as ligand.

The TG/DTG curves (Fig. 5a) show a mass loss step at the range 25–90 °C, connected with the possible evaporation of water, similar to that observed in the thermogram of zinc hexacyanocobaltate(III) (TG/DTG curves in Fig. 3).

Contrary to expectations, resulting from the use of a single pure compound (*tert*-butanol), the TG/DTG curves in the range 110–400 °C manifest the features of a three-step mass loss. The distinguishing feature of this phenomenon is that the respective steps of evaporation take place over a wide range of temperatures, significantly exceeding the boiling point of *tert*-butanol (80 °C), which indicates several forms of bonding of this ligand.

In temperatures above 400 °C, hexacyanocobaltate is observed to decompose as described above. Interpretation of the observed phenomenon is made possible by FTIR analysis of the gaseous products of decomposition of the test material. Figure 6 shows the EGA-FTIR thermogram, prepared as for the item above.

The EGA-FTIR thermogram has the unexpected feature of having absorption bands in the wave number ranges 3120–2600 cm^{-1}, 1700–1200 cm^{-1} and 920–820 cm^{-1} with a strong maximum at 890 cm^{-1}, which are recognized as the 2-methylpropene spectrum and are located with respect to the temperature axis in a manner that corresponds to the respective mass loss effects in the TG/DTG curve (the steps denoted by the numbers 1, 2, 3).

A simultaneous occurrence in the above temperature ranges of the absorption maxima which are characteristic for water (steps 1, 2, 3) convergent in shape and location as those for the maxima of 2-methylbutene, suggests that the effect has been caused by thermal decomposition with dehydration of *tert*-butanol, in accordance with Scheme C:

$$(CH)_3C - OH \xrightarrow{DMC} CH_2 = C(CH_3) - CH_3 + H_2O$$

Scheme C

Although the above reaction is known, it runs at temperatures above 400 °C in non-catalytic conditions [25]. Considering the DMC catalyst active site could act as a strong Lewis acid (Zn atoms) the promotion of the dehydration of *t*-BuOH would be justifiable. Particularly noteworthy is the occurrence of signals specific to the liberation of 2-methylpropene already during the first step of mass loss, which occurs at low temperatures (step 1 in the range 80–150 °C). This suggests that a possible decomposition of the catalyst-ligand complex may take place during or before the commencement of alcoxylation, which occurs typically at temperatures in the range 130–180 °C.

The above observation seriously suggests the necessity to revise the belief in the postulated mechanism of catalytic activity of DMC, according to which the ligand

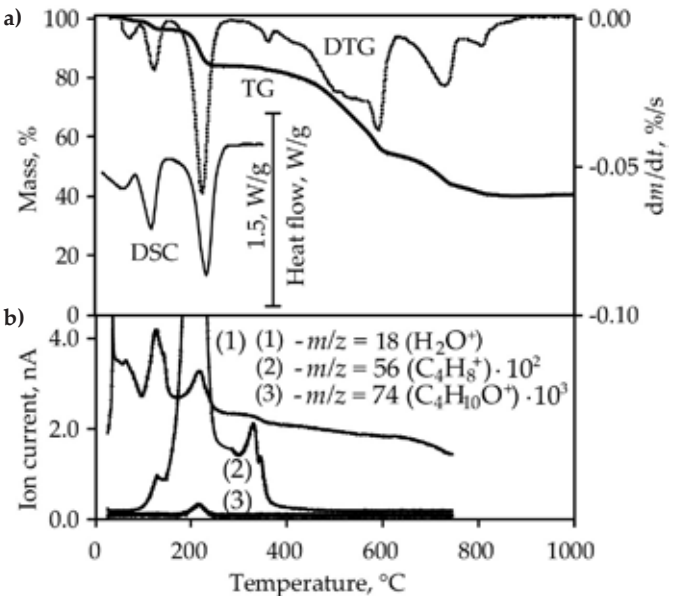

Fig. 5. Thermograms of DMC-*t*-BuOH catalyst: a) TG/DTG and DSC, b) EGA-MS

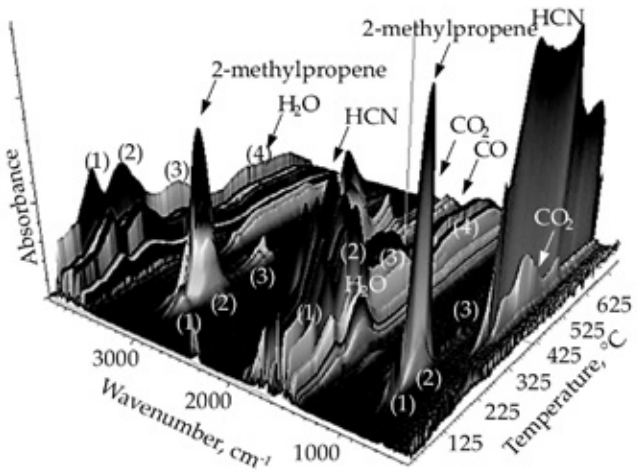

Fig. 6. EGA-FTIR thermogram of DMC-*t*-BuOH catalyst

is substituted with a propylene oxide molecule [4, 8, 9].

The process of liberation/decomposition of *tert*-butanol ends with the last, minor step (3) in the range 260––350 °C, and is followed by decomposition of the inorganic phase of the catalyst, which is accompanied by the evolution of identified components, described in the previous paragraph.

The course of the DSC curves for Fig. 5a conforms the adopted interpretation. In the temperature regions corresponding to the observed mass losses, the corresponding endothermal effects, connected with the decomposition processes, as suggested above, take place. The locations of the respective endothermic peaks correspond to the respective steps of mass loss visible in TG curves.

An additional EGA-MS analysis was performed in order to make more specific the above-proposed interpretation of the thermogram of the DMC catalyst containing *tert*-butanol as the ligand. Figure 5b shows the curves for the ionic currents corresponding to three selected molecular ions being formed in the course of fragmentation ionization of *tert*-butanol (*m*/*z* = 74), water (*m*/*z* = 18), and 2-methylpropene (*m*/*z* = 56).

In the case of curve 2, representing the ionic current of the molecular ion $C_4H_8^+$, three maxima were observed, being located in the temperature axis corresponding to the effects observed in the TGA and DSC curves and discussed above. The presence of the three characteristic maxima of the ionic current of $C_4H_{10}^+$ is accompanied by the occurrence of the respective ionic current strength maxima for *m*/*z* = 18 (curve 1), which confirms that water is generated along with the liberation of 2-methylbutene. Furthermore, the occurrence of low-strength ionic current of the molecular ion $C_4H_{10}O^+$ was detected (curve 3), indicating incomplete dehydration of *tert*-butanol in the

T a b l e 4. Values of quantitative characteristics of TG-curves steps (samples DMC-0—DMC-5)

Sample	TG mass loss steps, %					m_{res}	$[H_2O]^{TG}$ wt %	$[L]^{TG}$ wt %	$[L]^{cal}$ wt %
	20–90, °C	90–180, °C	180–280, °C	280–350, °C	350–1000, °C				
DMC-0	21.56	1.89 (90–350 °C)			39.96	36.55	21.56	0.00	0.04
DMC-1	3.31	4.32	9.47	2.50	39.62	40.78	3.31	16.29	14.89
DMC-2	3.53	3.78	9.65	2.38	40.61	40.05	3.53	15.81	16.04
DMC-3	1.28	3.00	11.05	1.17	42.82	39.51	1.28	15.22	13.65
DMC-4	0.43	1.05	10.24	0.00	29.50	58.78	0.43	11.29	12.89
DMC-5	8.38	7.22	2.55	1.63	47.21	33.01	8.38	11.4	10.73
Average	3.39	3.87	8.59	1.54	39.95	42.43	3.39	14.00	13.64
St. dev.	3.09	2.24	3.43	1.02	6.53	9.66	3.09	2.46	2.02
CV, %	91.20	57.92	39.96	66.26	16.35	22.76	91.20	17.53	14.82

m_{res} – TG residual mass after thermal decomposition;

$[H_2O]^{TG}$ – concentration of water in DMC material determined by TG, wt %;

$[L]^{TG}$ – concentration of ligand in DMC material determined by TG, wt %;

$[L]^{cal}$ – concentration of ligand in DMC material, as calculated from the stoichiometric balance of total carbon, wt %.

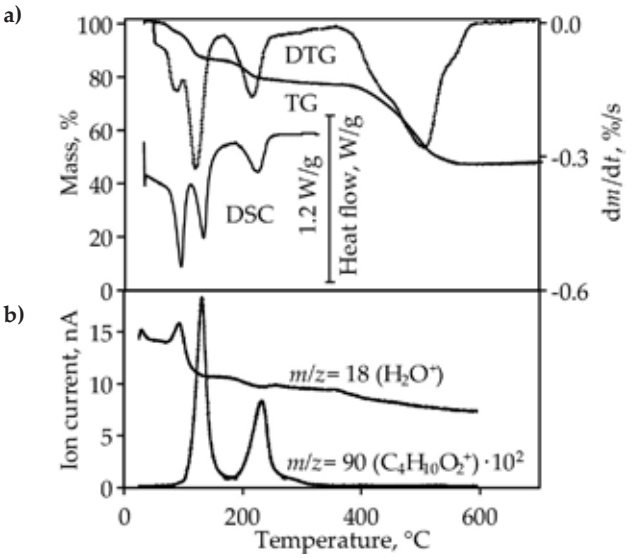

Fig. 7. Thermograms of DMC-glyme catalyst: a) TG/DTG and DSC, b) EGA-MS

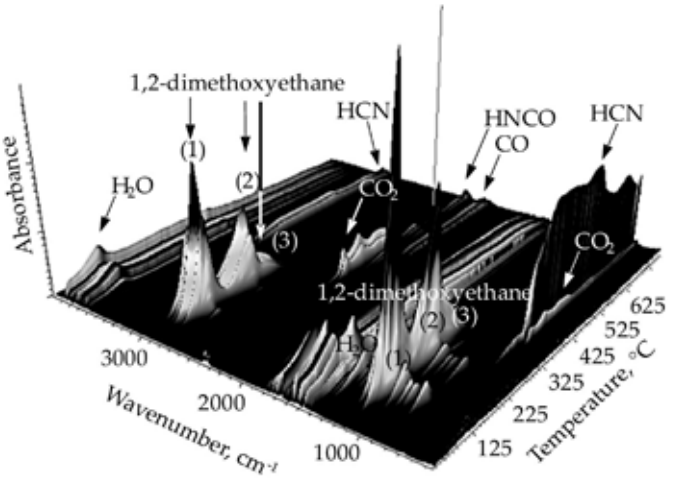

Fig. 8. EGA-FTIR thermogram of DMC-glyme catalyst

course of thermal decomposition of the test DMC catalyst and its partial evaporation.

The values of mass losses for the test DMC-*t*-BuOH catalysts, which occur in certain temperature ranges, are shown in Table 4.

DMC-glyme catalysts (DMC-6–DMC-10)

Thermograms of the DMC catalysts obtained with the use of 1,2-dimethoxyethane as an intentional ligand are shown in Fig. 7 and Fig. 8.

Among the identified mass loss steps which are observed in the TG/DTG curves in Fig. 7a, the step of water evaporation (which is known) in the range 25–90 °C can be distinguished along with two steps of evaporation of the volatile ligand: the first step is in the range 90–180 °C and the second is in the range 180–360 °C. Assuming that 1,2-dimethoxyethane is rather highly volatile (boiling point 85 °C), it should be noted that both mass loss steps that are connected with the evaporation of 1,2-dimethoxyethane are shifted significantly toward high temperatures, potentially indicating that dimethoxyethane is chemically bonded.

Similarly, in the case of zinc hexacyanocobaltate(III) and the DMC-*t*-BuOH catalysts discussed earlier, steps of decomposition of the inorganic part of the catalyst are observed at temperatures above 350 °C.

An explanation of the nature of thermal decomposition of the test materials is made possible by interpretation the EGA-FTIR thermograms shown in Fig. 8. A single maximum, connected with the appearance of water in gaseous products of decomposition of the weighed amount is observed at temperatures in the range 25––130 °C and in the wave number ranges 4000–3500 cm^{-1} and 2000–1300 cm^{-1}.

Moreover, above approx. 60 °C in the wave number ranges 3100–2700 cm^{-1} corresponding to stretching vibrations ν(C-H) there occur three maxima, identified as ones derived from elements of the structure of 1,2-dimethoxyethane.

The explanation is confirmed by the appearance, in the wave number range 1200–1050 cm^{-1}, of intense absorption maxima which are specific to the deformation vibrations of ether bonds C-O-C. The profile of the surface of the absorption function with respect to the temperature axis corresponds to the location of the respective mass losses observed in the TG/DTG thermograms.

In the temperature range above 300 °C, maxima which are specific to the decomposition processes observed in the cases discussed earlier occur.

The interpretation is supported by an EGA-MS analysis (Fig. 7b). The curve of the ion current, measured for the channel of $m/z = 18$ specific to the H_2O^+ ion, shows its characteristic increase in the temperature range corresponding to the first TG mass loss step and the appropriate strongly endothermal DSC peak (with a high value of water evaporation enthalpy) in the range of 50–90 °C. This expected effect confirms the nature of the TG/DSC stage as liberation of water existing in the DMC catalyst in the form of both a weakly bonded moisture and crystalline water.

In the curve that describes changes in the ion current for the molecular ion $C_4H_{10}O_2^+$ corresponding to the first step of ionization of 1,2-dimethoxyethane, the first peak connected with the liberation of that ligand does not appear until 100 °C.

Being more volatile than water (boiling point = 85 °C), the above mentioned component, if non bonded with any other physical or chemical forces stronger than associative liquid components, is evolved in the range of relatively low temperatures. The DSC curves of the pure glyme evaporation, published by Ponrouch *et al.* [26], demonstrate that the complete evaporation of pure liquid phase glyme occurs at temperatures in the range 50–100 °C.

The curve of glyme molecular ion current shows that the whole amount of the compound is liberated at much

T a b l e 5. Values of quantitative characteristics of TG-curves steps (samples DMC-6—DMC-10)

Sample	TG mass loss steps, %				m_{res}	$[H_2O]^{TG}$ wt %	$[L]^{TG}$ wt %	$[L]^{cal}$ wt %
	20–90, °C	90–180, °C	180—350, °C	350—1000, °C				
DMC-6	3.85	10.70	8.73	30.58	46.14	3.85	19.43	19.30
DMC-7	6.03	10.23	6.09	32.99	44.66	6.03	16.32	16.40
DMC-8	4.75	11.62	10.05	32.47	41.11	4.75	21.67	21.30
DMC-9	7.07	12.21	4.70	33.68	42.34	7.07	16.91	17.27
DMC-10	6.17	13.98	3.98	32.87	43.01	6.17	17.96	17.59
Average	5.57	11.75	6.71	32.52	43.45	5.57	18.46	18.37
St. dev.	1.27	1.47	2.60	1.17	1.97	1.27	2.15	1.95
CV, %	22.79	12.49	38.80	3.59	4.55	22.79	11.64	10.59

higher temperatures than it occurs in the case of a purely liquid phase: the first step in the range 100–180 °C, then the second in the range 180–300 °C with a small third one, overlapped near 300 °C. Since the maximum of DTG, DSC of glyme evaporation steps are shifted in relation to the pure liquid phase, one should expect that the most probable reason for that phenomenon is the bonding of glyme with coordination chemical forces, then the DSC effect observable in the described range of temperature could be the result of thermal dissociation of a DMC–glyme complex. Due to the fact that EXAFS analysis discovered the increase of the number of oxygen atoms around Co in distance 3.10 Å and 4.62 Å in catalysts as compare to reference hydrated material the ligand can be bounded close to Co atoms.

Quantitative thermal analysis of DMC materials

The results of quantitative assessment of the values of respective mass losses for the DMC test materials are shown in Tables 4 and 5.

The temperature ranges corresponding to the respective TG mass losses were determined from the temperature coordinates of local minima of the mass loss rates. The measures of the location and dispersion were described by means of suitable descriptive statistics, such as average, standard deviation for sample, and variability coefficient.

Since particular attention was paid to the temperature range where the volatile ligands which determine the catalyst's properties are liberated, the step of decomposition of the inorganic part was not described in detail; instead, quantitative assessment was generalized to the single step of thermal decomposition processes, which was running in the range 350 °C–1000 °C.

The values for mass loss steps exhibit significant dispersion. In spite of rather uniform elemental composition, the values of percentages of the individual mass losses vary to a considerable extent; this is especially applicable to water content and the mass loss percentages connected with liberation/decomposition of ligands. A significantly higher repeatability of results is observed for quantitative characteristics connected with decomposition of the inorganic part of the catalyst.

In order to confirm the working hypothesis that the TG/DSC curve steps above 90 °C are connected entirely with the liberation of ligands, the stoichiomertric mass balance of both ligands was performed on the basis of an independently conducted elemental analysis.

If one made the justified assumption that the total nitrogen determined must correspond solely to the cyanide groups bonded with cobalt in a particularly stable $[Co(CN)_6]^{3-}$ complex ion, the difference between the cyanide stoichiometric carbon and the total carbon would result from the presence of the ligand. Thus, the calculation of the ligand content in DMC could be possible, using the following stoichiometric Eq. 1:

$$[L]^{cal} = \frac{[C] - \frac{M_C}{M_N} \cdot [N]}{[C]_L} \quad (1)$$

where: [C] – total carbon concentration in DMC material, wt %, $[C]_L$ – total carbon concentration in organic ligand, wt %, [N] – total nitrogen concentration in DMC material, wt %, $[L]^{cal}$ – concentration of ligand in DMC material, as calculated from the stoichiometric balance of total carbon, wt %, M_C – molar mass of carbon, g/mol, M_N – molar mass of nitrogen, g/mol.

The values of the TG percent mass loss corresponding to the whole ligand liberation TG stage ($[L]^{TG}$) and the concentration of the ligand, calculated stoichiometrically from Eq. (1), were put down in Tables 4 and 5.

The correlation between $[L]^{TG}$ and $[L]^{cal}$ occurred to be the linear and could be described with the Eq. (2):

$$[L]^{TG} = 0.9844 \cdot [L]^{cal} \quad (2)$$

where: $[L]^{TG}$ – concentration of ligand in DMC material, as determined by TG, wt %.

The value of the regression coefficient is close to unity (0.9844) while that of the linear correlation coefficient is relatively high ($r \approx 0.99$), indicating that the adopted quantitative interpretation is correct.

CONCLUSIONS

Thermoanalytical studies of the DMC test materials indicate that their thermal decomposition is a multi-step

process. The results of EGA-FTIR and EGA-MS analyses enabled identification of the physical-chemical nature of the decomposition processes observed. The studies have shown that the course of decomposition of the DMC catalysts comprises generally two steps: liberation of moisture along with volatile ligands which takes place in the range 25–400 °C and decomposition of the inorganic part which occurs in the range 400–~ 700 °C. Above 700 °C, the decomposition residue is constant.

Surprisingly, the volatile ligands were found to be liberated at much higher temperatures than those expected from the volatilities of such compounds, and the liberation process consists of multiple steps, indicating ligand bonding into compounds having different stabilities. Specifically, in the case of the DMC catalyst based on *tert*-butanol, it was found that dehydration of the ligand is accompanied by formation of 2-methylbutene and water. This is an particularly interesting phenomenon because it begins at rather low temperatures of approx. 120 °C, although this known reaction in non-catalytic conditions requires temperatures of about 400 °C. Considering that Zn is acting as a Lewis acid, coordinated to the oxygen atom of *t*-BuOH, dehydration should be strongly favored (as it takes place in a catalyzed manner) over the simple thermal process. In the case of DMC catalysts obtained with the use of 1,2-dimethoxyethane, also ligand liberation was observed to be taking place in multiple steps. This indicates ligand bonding into compounds having different stabilities, although decomposition of 1,2-dimethoxyethane was not taking place.

The present study on the relationships between the ligand content as found by TG and its content resulting from the stoichiometric balance for total carbon, as found by elemental analysis, indicate satisfactory correlations which are sufficient for the quantitative determination of the ligand by TG.

The course of thermal decomposition of the inorganic part of the DMC test materials was similar and was accompanied mainly by hydrogen cyanide and carbon dioxide emissions.

The local atomic order around Zn atoms as resulted from the EXAFS analysis support the model of active catalytic center proposed by Zhang *et al*. [8] on the base of XPS and IR spectroscopy and the model resulting from molecular calculation performed by Wojdeł *et al*. [22]. These models assume the important role of Zn-Cl bonds in the activity of DMC class of catalysts. The role of Zn-O bond postulated in other papers is not confirmed by EXAFS studies. No next Zn atom was detected in the distance 4.38 Å from Zn as resulted from calculation performed in [23]. Therefore, we postulate that catalysts form cluster-like complexes with the Co local atomic structure not affected, as compared to reference cubic hydrated material in $[Co(CN)_6]^{3-}$ ion. The Zn atoms inside the clusters have changed atomic order which becomes like in anhydrous structure (tetrahedral coordination). This explains that part of Zn atoms having an atomic order similar to that in the reference anhydrous material. Remaining Zn atoms can be located at the surface of the clusters and bound partially with groups of cyanide and with chlorine atoms. These surface Zn atoms can be catalyst active centers. EXAFS analysis does not confirmed the existence of $ZnCl_2$ compounds in catalyst. Therefore, the direct evidence was given that formula $Zn_3[Co(CN)_6]_2{\cdot}xZnCl_2{\cdot}yL$ used to describe DMC catalyst is not valid. Instead the disordered nanoclusters are formed in catalyst with different atomic order around Co and Zn with new, unknown structure, which incorporates Cl atoms.

ACKNOWLEDGMENT

The research was funded by the Polish National Centre for Research and Development Project Innotech K2/IN2/21/181982/NCBR/ 12(K-DMC).

REFERENCES

[1] Bailey F.E., Koleske J.V.: "Surfactant Science Series", Vol. 35, Marcel Dekker, Inc., New York and Basel, 1991.
[2] Ionescu M.: "Chemistry and Technology of Polyols for Polyurethanes", R.A.P.R.A. Technology Ltd. Shawbury-Shrewsbury-Shropshire, UK 2005.
[3] Chruściel A., Hreczuch W., Janik J. *et al*.: *Industrial and Engineering Chemistry Research* **2014**, *53*, 6636. http://dx.doi.org/10.1021/ie500031j
[4] Kim I., Ahn J.-T., Ha Ch.-S. *et al*.: *Polymer* **2003**, *44*, 3417. http://dx.doi.org/10.1016/S0032-3861(03)00226-X
[5] Chen S., Zhang P., Chen L.: *Progress in Organic Coatings* **2004,** *50*, 269. http://dx.doi.org/10.1016/j.porgcoat.2004.03.003
[6] Kim I., Byun S.H., Ha C.S.: *Journal of Polymer Science Part A: Polymer Chemistry* **2005,** *43*, 4393. http://dx.doi.org/10.1002/pola.20914
[7] Lee S., Baek S., Anas T.K. *et al*.: *Polymer* **2007,** *48*, 4361. http://dx.doi.org/10.1016/j.polymer.2007.05.072
[8] Zhang X.-H., Hua Z.-J., Chen Sh. *et al*.: *Applied Catalysis A: General* **2007**, *325*, 91. http://dx.doi.org/10.1016/j.apcata.2007.03.014
[9] Huang Y.-J., Zhang X.-H., Hua Z.-J. *et al*.: *Macromolecular Chemistry and Physics* **2010**, *11*, 1229. http://dx.doi.org/10.1002/macp.200900666
[10] van der Kerk G.J.M.: *Pure and Applied Chemistry* **1972**, *30* (*3–4*), 389. http://dx.doi.org/10.1351/pac197230030389
[11] Wells A.F.: "Structural Inorganic Chemistry Oxford University Press", 1984.
[12] Huang Y.J., Qi G.R., Chen L.Sh.: *Applied Catalysis A: General* **2003**, *240*, 263. http://dx.doi.org/10.1016/S0926-860X(02)00452-0
[13] Liu H., Wang X., Gu Y., Guo W.: *Molecules* **2003**, *8*, 67. http://dx.doi.org/10.3390/80100067
[14] Kim I., Ahn J.-T., Lee S.-H. *et al*.: *Catalysis Today* **2004**, *93*, 511. http://dx.doi.org/10.1016/j.cattod.2004.06.001
[15] Yoon J.H., Lee I.K., Choi H.Y. *et al*.: *Green Chemistry* **2011**, *13*, 631.

http://dx.doi.org/10.1039/c0gc00554a
[16] Lawniczak-Jabłońska K., Demchenko I., Dynowska E. *et al*.: *Acta Crystallographica* **2014**, *A70*, C592. http://dx.doi.org/10.1107/S2053273314094078
[17] Lawniczak-Jabłonska K., Dynowska E., Lisowski W. *et al*.: *X-ray Spectrometry* **2015**, *44*, 330. http://dx.doi.org/10.1002/xrs.2636
[18] Sebastian J., Srinivas D.: *Applied Catalysis A: General* **2014**, *482*, 300. http://dx.doi.org/10.1016/j.apcata.2014.06.007
[19] Lee I.K., Ha J.Y., Cao Ch. *et al*.: *Catalysis Today* **2009**, *148*, 389. http://dx.doi.org/10.1016/j.cattod.2009.07.073
[20] Šutinska V., Patjášová M., Ondrušová D. *et al*.: *Journal of Thermal Analysis and Calorimetry* **2011**, *104*, 923. http://dx.doi.org/10.1007/s10973-011-1314-2
[21] Zhou T., Zou Zh., Gan J. *et al*.: *Journal of Polymer Research* **2011**, *18*, 2071. http://dx.doi.org/10.1007/s10965-011-9616-4
[22] Wojdeł J.C., Bromley S.T., Illas F., Jansen J.C.: *Journal of Molecular Modeling* **2007**, *13*, 751. http://dx.doi.org/10.1007/s00894-007-0218-3
[23] Almora-Barrios N., Pogodin S., Bellarosa L. *et al*.: *ChemCatChem Catalysis* **2015**, *7*, 928. http://dx.doi.org/10.1002/cctc.201402907
[24] Rodríguez-Hernández J., Reguera E., Lima E. *et al*.: *Journal of Physics and Chemistry of Solids* **2007**, *68*, 1630. http://dx.doi.org/10.1016/j.jpcs.2007.03.054
[25] Barnard J.A.: *Transactions of the Faraday Society* **1959**, *55*, 947. http://dx.doi.org/10.1039/tf9595500947
[26] Ponrouch A., Marchante E., Courty M. *et al*.: *Energy and Environmental Science* **2012,** *5*, 8572. http://dx.doi.org/10.1039/c2ee22258b